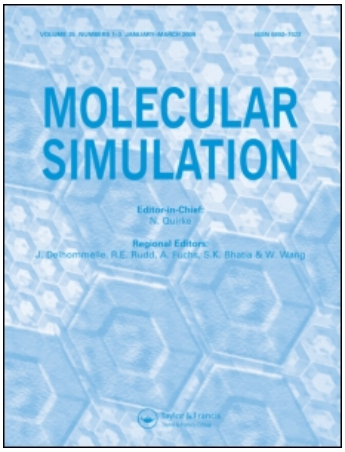

Molecular Simulation
Publication details, including instructions for authors and subscription information:
http://www.informaworld.com/smpp/title~content=t713644482

Calculations on cyclopyranoses as co-solvents of single-wall carbon nanotubes

Francisco Torrens[a]
[a] Institut Universitari de Ciència Molecular, Universitat de València, Burjassot(València), Spain

To cite this Article Torrens, Francisco(2005) 'Calculations on cyclopyranoses as co-solvents of single-wall carbon nanotubes', Molecular Simulation, 31: 2, 107 — 114
To link to this Article: DOI: 10.1080/08927020412331308494
URL: http://dx.doi.org/10.1080/08927020412331308494

Molecular Simulation, Vol. 31, No. 2–3, 15 February–15 March 2005, 107–114

Taylor & Francis
Taylor & Francis Group

Calculations on *cyclo*pyranoses as co-solvents of single-wall carbon nanotubes

FRANCISCO TORRENS*

Institut Universitari de Ciència Molecular, Universitat de València, Dr. Moliner 50, E-46100 Burjassot (València), Spain

(Received March 2004; in final form June 2004)

The properties of single-wall carbon nanotubes (SWNT) are classified in *zigzag* $(n,0)$, *armchair* (n,n) and *chiral* (n,m). The solubility of SWNTs is investigated in a variety of solvents, finding a class of non-hydrogen-bonding Lewis bases that provide a good solubility. The investigated solvents are grouped into three classes. Categorized solubility is semiquantitatively correlated with solvent parameters. A MOPAC-AM1 and molecular modelling study of the linear and cyclic (**1** → **4**)-linked oligosaccharides containing 1–6 D-glucopyranose (D-Glc*p*) units provides a clear conception of their overall conformations, their contact surfaces and their cavity proportions. This gives a first estimation of their inclusion properties. An expansion of the central channel is suggested for helical D-Glc*p*–SWNT complexes.

Keywords: Carbon nanotube; Solvation parameter model; Partition coefficient; Relative dielectric permittivity; Electron affinity; Hydrophobicity pattern

ACS Classification Codes: Colloids (Physicochemical Aspects); Detergents; Soaps; Surfactants; Solvent extraction

1. Introduction

Since their discovery in 1993 [1], single-wall carbon nanotubes (SWNT) have found numerous applications [2] in chemistry and physics because of their anisotropic shapes (diameters of around 1 nm and lengths of micrometers), remarkable strengths and elasticities, and unique physical properties, e.g. high thermal and electrical conductivities. By contrast, and despite their clear potential, SWNTs have not yet been fully integrated into biological systems [3], mainly because of the considerable difficulty in rendering them soluble in aqueous solutions.

Initially, the challenge of achieving soluble SWNTs in organic solvents was addressed by their covalent modification (examples include both end-group [4] and side-wall [5] functionalization). Covalent modification, however, has the disadvantage that it impairs their physical properties. For these and other reasons, we have been attracted by a supramolecular approach [6] to the solubilization problem (namely, the noncovalent functionalization of SWNTs by wrapping polymers around them in the knowledge that desired features can be grafted onto the polymers, before their being self-assembled around the SWNTs). Considerable progress [7] was made in the use of synthetic polymers to render SWNTs soluble in organic solvents. However, while some water-soluble polymers [8] and surfactants [9] can bring aqueous solubilities to SWNTs, they may not be as biocompatible as would be desirable.

It was for this reason, amongst others, that Stoddart's group decided to explore the possibility of solubilizing SWNTs in aqueous solutions of starch [10]. They knew from their knowledge of the supramolecular chemistry of fullerenes [11] that cyclodextrins (CD) of the appropriate dimensions [CD_8 (γ-CD) commonly and CD_9 (δ-CD) occasionally], and in the correct stoichiometries, will dissolve fullerenes (e.g. C_{60} and C_{70}) in water [12]. CDs are the macrocyclic analogues [13] of starch. The connection is clear. They reported that [14]: (1) common starch, provided it is activated towards complexation by wrapping itself helically around small molecules, will transport SWNTs competitively to aqueous solutions, (2) the process is sufficiently reversible at high temperatures to permit the separation of SWNTs in their supramolecular starch-wrapped form by a series of physical manipulations from amorphous carbon, and (3) the addition of glucosidases to these starched carbon nanotubes results in the precipitation of the SWNTs from aqueous solution.

*E-mail: francisco.torrens@uv.es

Molecular Simulation
ISSN 0892-7022 print/ISSN 1029-0435 online © 2005 Taylor & Francis Group Ltd
http://www.tandf.co.uk/journals
DOI: 10.1080/08927020412331308494

The naturally occurring cyclodextrins CD_{6-9} (α–δ-CD) are a group of cyclic oligosaccharides containing 6–9 α-(1 → 4)-linked D-glucopyranose (D-Glc*p*) units per molecule, which have unusual loop structures (a feature that allows them to form inclusion complexes by insertion of a wide variety of organic molecules into their hydrophobic intramolecular cavity [15]). For D-Glcp_{1-6}, this study provides a first assessment of their conformational and lipophilic features.

In earlier publications, periodic tables (PT) of fullerenes [16,17] and SWNTs [18,19] were discussed. A program based on the AQUAFAC model was applied to calculate the aqueous coefficients of SWNTs [20]. The present study is an attempt to elucidate the solvation of SWNTs in the hopes of pointing the way towards better solvents. Some solvation and partition properties for D-Glcp_n are computed. Section 2 presents the methods. Following that, the results are discussed in Section 3. The last section summarizes the conclusions.

2. Materials and methods

2.1 Program TOPO

TOPO [21] represents the surface of molecules by the external surface of a set of overlapping spheres with appropriate radii [22], centered on the nuclei of the atoms [23]. The molecule is treated as a solid in space defined by tracing spheres about the atomic nuclei. It is enclosed in a box and the geometric descriptors evaluated counting points within the solid or close to chosen surfaces. The molecular volume is calculated as $V = P \times \mathrm{GRID}^3$, where P is the number of points within the molecular volume and GRID is the size of the mesh grid. The molecular *bare* surface area could be estimated as $S = Q \times \mathrm{GRID}^2$, where Q is the number of points close to the bare surface area (within a distance between R_X and $R_X + \mathrm{GRID}$ of any atomic nucleus X). If the point falls exactly on the surface of one of the atomic spheres, it accounts for GRID^2 units of area on the molecular bare surface. This is because the total surface of atom X can accommodate $4\pi R_X^2/\mathrm{GRID}^2$ points. When a point falls beyond the surface, it represents GRID^2 units of area on the surface of a sphere of radius $R > R_X$, not on the surface of atom X. On the surface of X, it accounts for only a fraction of the quantity $\mathrm{GRID}^2(R_X/R)^2$. The total bare surface area is calculated now as $S = F \times \mathrm{GRID}^2$, where F is the sum of elements AF defined as $\mathrm{AF} = R_X^2/R^2(I)$ for those points close enough to the surface of any atom X. R_X^2 is the squared radius of atom X and $R^2(I)$ is the squared distance of point I from the atomic nucleus X. If S_e is the surface area of a sphere whose volume is equal to the molecular volume V, the ratio $G = S_e/S$ is interpreted as a descriptor of molecular *globularity*. The ratio $G' = S/V$ is interpreted as a descriptor of molecular *rugosity*. The solvent-accessible surface (AS) is calculated in the same way as S via pseudoatoms, whose van der Waals radii are increased by the radius R of the probe. The *fractal-like index* D of the molecules [24] is obtained as

$$D = 2 - \frac{\mathrm{d}(\log \mathrm{AS})}{\mathrm{d}(\log R)} \tag{1}$$

where R is the probe radius [25]. The difference with latest version of TOPO (2004) is that the latter includes an actualized database of van der Waals radii [26]. TOPO has been implemented in programs AMYR [27], SURMO2 [28] and GEPOL [29].

2.2 Program SCAP

SCAP [30–35] is an extension of the solvent-dependent conformational analysis program 1-octanol–water model to other organic solvents [36]. SCAP is based on the model of Hopfinger parameterized for the 1-octanol–water solvent pair with solute molecules composed of H, C, N, O, F, S, Cl and Br, and containing a wide variety of functional groups. SCAP was initially used to calculate the Gibbs free energy of solvation of molecules. From these data and with the equation

$$RT \ln P = \Delta G^{\mathrm{o}}_{\mathrm{solv}}(\mathrm{water}) - \Delta G^{\mathrm{o}}_{\mathrm{solv}}(1-\mathrm{octanol}) \tag{2}$$

one can calculate the logarithm $\log P$ at a given T which is taken as 298 K. R is the gas constant, and $\Delta G^{\mathrm{o}}_{\mathrm{solv}}$ (1 – octanol) and $\Delta G^{\mathrm{o}}_{\mathrm{solv}}$(water) are the standard-state free energies of solvation of a given solute considered in 1-octanol and water, respectively.

For a general organic solvent, e.g. cyclohexane, the maximum number of solvent molecules allowed to fill the solvation sphere is related to the volume of the solvent molecule as

$$n_{\mathrm{s}} = n_{\mathrm{o}} \left(\frac{V_{\mathrm{s,s}}}{V_{\mathrm{s,o}}} \right)^{\log \frac{n_{\mathrm{o}}}{n_{\mathrm{w}}} / \log \frac{V_{\mathrm{s,o}}}{V_{\mathrm{s,w}}}} \tag{3}$$

where V_{s} is the volume of the solvent molecule, and the subscripts o, w and s stand for 1-octanol, water and a general organic solvent, respectively.

The variation in the standard Gibbs free energy associated with the extraction of one solvent molecule out of the solvation sphere $\Delta g^{\mathrm{o}}_{\mathrm{s}}$ is calculated using the generalized Born equation [37],

$$\Delta g^{\mathrm{o}}_{\mathrm{s}} = \Delta g^{\mathrm{o}}_{\mathrm{o}} \frac{1 - (1/\varepsilon_{\mathrm{s}})}{1 - (1/\varepsilon_{\mathrm{o}})} = \Delta g^{\mathrm{o}}_{\mathrm{o}} \frac{\varepsilon_{\mathrm{o}}(\varepsilon_{\mathrm{s}} - 1)}{\varepsilon_{\mathrm{s}}(\varepsilon_{\mathrm{o}} - 1)} \tag{4}$$

where ε_{o} and ε_{s} are the relative dielectric constants. Previous results for benzene suggested a variation of only 80% of that (equation (4)) [30]. However, the calculation of more molecules showed that it is a better rule to expand this variation up to 100% [31].

The radius of the solvation sphere is related to the volume of the solvent molecule as

$$R_{\mathrm{v,s}} = R_{\mathrm{v,o}} \left(\frac{V_{\mathrm{s,s}}}{V_{\mathrm{s,o}}} \right)^{1/3} \tag{5}$$

Finally, the free volume available for a solvent molecule in the solvation sphere is related to the volume of the solvent molecule as

$$V_{f,s} = V_{f,o}\frac{V_{s,s}}{V_{s,o}} \quad (6)$$

The only parameters needed are the relative dielectric constant ε and molecular volume V_s of the organic solvent. V_s values have been calculated with TOPO 2004. In the present work, the following values have been used: $\varepsilon = 9.862$, 2.023 and 4.806 [38]; $V_s = 155.0$, 93.4 and 72.1 Å^3 for 1-octanol, cyclohexane and chloroform, respectively.

2.3. Program CDHI

The 1-octanol–water partition coefficient $\log P_o$ has been obtained with a method developed by Kantola *et al.* [39] for the computation of conformationally dependent hydrophobic indices based on atomic contributions. The method uses the following expression for the 1-octanol–water partition coefficient:

$$\log P_o = \sum_i \alpha_i(N)S_i + \beta_i(N)S_i(\Delta q_i)^2 + \gamma_i(N)\Delta q_i \quad (7)$$

where S_i is the contribution of atom i to the molecular surface area; Δq_i is the total atomic charge [40,41]; and α_i, β_i and γ_i are fitting parameters dependent only on the atomic number of atom i. A program called CDHI has been written. An atom–atom partition analysis of $\log P_o$ has been implemented near selected atoms. The contribution of each atom to the molecular surface area is calculated with TOPO. The net atomic charges Δq have been computed with program POLAR, which has been described elsewhere [42]. Notice that the comparison between SCAP and CDHI has a special interest. The latter assigns a set of fitted parameters for each atom depending only on its atomic number and not on the surrounding atoms in the molecule. Instead, SCAP also takes into account the functional group to which each atom in the molecule belongs. Our programs are available from the author and are free for academics.

3. Results and discussion

Although solubility in organic solvents is predicted rather greater than in water (logarithm of the organic solvent–water partition coefficient $\log P \gg 1$), the absolute solubility in organic solvents is also estimated to be extremely small [e.g. $S_{cf(10,10)} \approx P_{cf} \times S_w = 10^{53.6} \times 10^{-92.4} = 10^{-38.8} < 10^{-23}$ mol L^{-1}, where S_{cf} and S_w are the solubilities in chloroform ($CHCl_3$) and water, respectively, and P_{cf} is the $CHCl_3$–water partition coefficient [20]. Therefore, no solute molecule would be present in solution. The results are consistent with the experimental observation that there are rather few good solvents for SWNTs. Toluene, ethanol, isopropyl alcohol and acetone do not dissolve SWNTs. However, $CHCl_3$ keeps SWNTs in more or less stable suspension for days. It is suggested that most other chlorinated solvents, e.g. *ortho*-dichlorobenzene (ODCB) behave similarly. The solvochromic parameters (α, β and π^*), relative dielectric permittivity ε, semiempirical MOPAC-AM1 [43] ionization potential I, electron affinity (EA), TOPO molecular volume V and suggested charge transfer for different solvents are listed in table 1. The studied conformations are minima optimized at the AM1 level of calculation.

The solvents can be divided into three groups. Class 1 consists of the *best* solvents, *N*-methylpyrrolidone (NMP), *N,N*-dimethylformamide (DMF), hexamethylphosphoramide (HMPA), cyclopentanone, tetramethylene sulfoxide and ε-caprolactone, which readily disperse SWNTs, forming light-grey, slightly scattering liquid phases [44]. These solvents are characterized by high values for electron-pair donicity β [45], negligible values for hydrogen-bond donation parameter α [46], and high values for solvochromic parameter π^* [47]. Lewis basicity (availability of a free electron pair) without hydrogen donors is a key to good solvation of SWNTs. As $\varepsilon \approx 33$ and EA ≈ -29 kJ mol^{-1}, it is suggested that SWNTs in these solvents have a partial negative charge due to the high β. Class 2 contains the *good* solvents, toluene, 1,2-dimethylbencene, carbon disulphide, 1-methylnaphthalene, iodobenzene, $CHCl_3$, bromobenzene and ODCB, known to be exceptional for C_{60-70} [48]. They show $\alpha \approx \beta \approx 0$, high π^*, $\varepsilon \approx 10$ and EA $\gg 0$. $CHCl_3$ and ODCB have similar ε and EAs and suspend SWNTs. Other solvents that are co-miscible with ODCB but that are a poor ε/EA match, e.g. *n*-hexane, do not suspend SWNTs. The results are in agreement with electroplating experiments which showed that SWNTs in ODCB and ODCB/$CHCl_3$ are positively charged [49]. However, SWNTs are not suspended in ODCB/*n*-hexane. These observations are attributed to the large EA of ODCB and the negative EA of *n*-hexane. It is suggested that SWNTs in $CHCl_3$ are positively charged due to the large positive EA of $CHCl_3$, and that SWNTs in other chlorinated solvents with large positive EA are also positively charged. By contrast, when SWNTs are suspended using certain nonionic surfactants (Triton X-100, a tensoactive used in biochemistry), colloids of negatively charged SWNTs are produced. Controllable aggregation of SWNTs is achieved diluting a SWNT/ODCB solution with $CHCl_3$. Greater aggregation (diluting SWNT/ODCB with *n*-hexane) causes complete precipitation of SWNTs. Class 3 entails the *bad* solvents, *n*-hexane, ethyl isothiocyanate, acrylonitrile, dimethyl sulfoxide (DMSO), water and 4-chloroanisole, with a poor ε-EA match with NMP or ODCB. It is suggested that SWNTs in these solvents have a partial positive charge provided EA > 0.

Triton X-100 [$C(CH_3)_3$—CH_2—$C(CH_3)_2$—C_6H_4—(O—CH_2—$CH_2)_n$—OH $n = 10$ (average)] has been included for comparison. Although the molecular volume is quantitatively different from class-1 compounds, it is also known to form colloids of negatively charged

Table 1. Solvochromic parameters, dielectric permittivity, ionization potential, electron affinity, volume and charge transfer for solvents.

Solvent/suspender	α*	β†	π*‡	ε¶	I§	EA‖	V#	Charge transfer
Cyclopentanone	0.000	0.537	0.756	16.30**	1041.5	−24.2	80.8	$SWNT^-/solvent^+$
Hexamethylphosphoramide (HMPA)	0.000	0.990	0.871	29.00	595.7	−44.7	162.9	$SWNT^-/solvent^+$
N-methylpyrrolidone (NMP)	0.000	0.754	0.921	32.58	820.8	−29.2	92.6	$SWNT^-/solvent^+$
N,*N*-dimethylformamide (DMF)	0.000	0.710	0.875	37.06	847.0	−44.2	70.9	$SWNT^-/solvent^+$
Tetramethylene sulfoxide	0.000	0.800	1.000	42.84	832.6	6.6	88.3	$SWNT^-/solvent^+$
ε-caprolactone	–	–	–	–	–	−12.3	103.1	$SWNT^-/solvent^+$
Mean	0.000	0.758	0.885	31.56	827.5	−24.7	99.8	$SWNT^-/solvent^+$
Toluene	0.000	0.110	0.535	2.379††	843.0	2.1	95.0	$SWNT^+/solvent^-$
1,2-Dimethylbenzene	0.000	0.120	0.510	2.568	–	6.1	110.4	$SWNT^+/solvent^-$
Carbon disulphide	0.000	0.070	0.514	2.641	864.4	129.2	55.5	$SWNT^+/solvent^-$
1-Methylnaphthalene	0.000	0.100	0.800	2.710	778.0	73.5	146.9	$SWNT^+/solvent^-$
Iodobenzene	0.000	0.050	0.810	4.630	–	63.8	105.9	$SWNT^+/solvent^-$
Chloroform ($CHCl_3$)	0.200	0.100	0.760	4.806	1084.8	108.1	72.1	$SWNT^+/solvent^-$
Bromobenzene	0.000	0.060	0.794	5.400††	–	43.4	98.1	$SWNT^+/solvent^-$
ortho-Dichlorobenzene (ODCB)	0.000	0.030	0.800	9.930††	854.9¶¶	71.5	110.3	$SWNT^+/solvent^-$
Mean	0.025	0.080	0.690	4.383	885.0	62.2	99.3	$SWNT^+/solvent^-$
n-Hexane	0.000	0.000	−0.081	1.890	1002.7	−290.9	103.5	$SWNT^-/solvent^+$
Ethyl isothiocyanate	–	–	–	19.50‡‡	814.6	101.7	80.1	$SWNT^+/solvent^-$
Acrylonitrile	–	0.250	0.870	33.01	991.4	44.4	57.1	$SWNT^+/solvent^-$
Dimethyl sulfoxide (DMSO)	0.000	0.752	1.000	46.71	832.8	17.8	66.8	$SWNT^+/solvent^-$
Water	1.017	0.470	1.090	80.37	1150.2	−332.3	23.8	$SWNT^-/solvent^+$
4-Chloroanisole	–	–	–	–	800.5	4.3	118.1	$SWNT^+/solvent^-$
Mean	0.339	0.368	0.720	36.30	932.0	−75.8	74.9	$SWNT^+/solvent^-$
Triton X-100	–	–	–	–	–	–	597.7	$SWNT^-/co\text{-}solvent^+$
12-Crown-4 ether	–	–	–	–	896.9	−70.6	155.6	$SWNT^-/co\text{-}solvent^+$
15-Crown-5 ether	–	–	–	–	851.6	−59.1	194.3	$SWNT^-/co\text{-}solvent^+$
18-Crown-6 ether	–	–	–	–	843.6	−115.3	232.9	$SWNT^-/co\text{-}solvent^+$
30-Crown-10 ether	–	–	–	–	–	–	388.1	$SWNT^-/co\text{-}solvent^+$

* Hydrogen-bond donation acidity. † Hydrogen-bond acceptance basicity. ‡ Solvochromic parameter. ¶ Relative dielectric permittivity at 20°C. § Ionization potential (kJ mol^{-1}) calculated with MOPAC-AM1. ‖ Electron affinity (kJ mol^{-1}) calculated with MOPAC-AM1. # Molecular volume ($Å^3$). ** At −51°C. †† At 25°C. ‡‡ At 21°C. ¶¶ Calculated with MOPAC-MNDO-d.

SWNTs in water. The polyether $(O—CH_2—CH_2)_n$ moiety of Triton X suggests to study 12-, 15-, 18- and 30-membered cyclic 3*n*-crown-*n* ethers [*cyclo*$(O—CH_2—CH_2)_n$]. The negative EAs of the crown ethers, e.g. $EA_{12-crown-4} = -70.6\,kJ\,mol^{-1}$, suggest the formation of colloids of negatively charged SWNTs in water. This is in agreement with the fact that crown ethers form complexes with metal cations in water.

The formal approach of quantitative structure–property relationships has been used. The solubility *S* is categorized as 1, 0 and −1 in arbitrary units for classes 1, 2 and 3, respectively. The values of *S*, ε, *I*, EA and *V* have been semiquantitatively correlated for the three classes. The best linear fit turns out to be:

$$S = 0.00679 + 0.00126EA \tag{8}$$

$$N = 18 \quad s = 0.774 \quad F = 0.7 \quad MAPE = 102.73\%$$

$$AEV = 0.9593$$

where MAPE is the mean absolute percentage error and AEV is the approximation error variance. All other models with greater MAPE and AEV have been discarded. The best quadratic model for *S* turns out to be:

$$S = 0.178 - 0.0000124EA^2 \tag{9}$$

$$N = 18 \quad s = 0.684 \quad F = 5.4 \quad MAPE = 88.01\%$$

$$AEV = 0.7486$$

and AEV decreases by 22%.

If α, β and π^* are included in the fit, the best linear model turns out to be:

$$S = -0.171 + 2.31\beta - 0.0274\varepsilon \tag{10}$$

$$N = 17 \quad s = 0.515 \quad F = 9.9 \quad MAPE = 65.28\%$$

$$AEV = 0.4146$$

and AEV diminishes by 57%. The best quadratic model for *S* turns out to be:

$$\begin{aligned} S &= 0.0588 + 0.605z_{12} - 0.272z_{11}z_{12} \\ z_{11} &= 0.0974 + 0.00832EA \\ z_{12} &= -0.737 + 13.9\beta - 13.2\beta\pi^* \quad N = 17 \end{aligned} \tag{11}$$

$$MAPE = 59.76\% \quad AEV = 0.4032$$

and AEV drops by 58%.

Correlation improves for smaller subsets. For instance, if only classes 1 and 2 are considered, the best linear model turns out to be:

$$S = 0.173 + 1.40\beta - 0.00267V \tag{12}$$

$$N = 13 \quad R = 0.974 \quad s = 0.125 \quad F = 94.0$$

$$MAPE = 21.60\% \quad AEV = 0.0505$$

and AEV diminishes by 95%.

The free energies of solvation and partition coefficients *P* of α-(1→4)-linked D-glc*p* residues have been

Table 2. Free energy of solvation and partition coefficient results for α-(1 → 4)-linked D-glucopyranose residues.

D-glucopyranose	$\Delta G_{solv,w}$*	$\Delta G_{solv,o}$†	$\Delta G_{solv,ch}$‡	$\Delta G_{solv,cf}$¶	log P_o§	log P_o Ref.‖	log P_{ch}#	log P_{ch} Ref.**	log P_{cf}††	log P_{cf} Ref.**
D-Glcp	−61.4	−37.5	−23.0	−37.8	−4.20	−6.50	−6.75	−5.20	−4.15	−5.19
[D-Glcp $\alpha(1\rightarrow4)]_2$	−101	−64.8	−39.3	−64.4	−6.32	−11.2	−10.8	−7.45	−6.38	−7.89
[D-Glcp $\alpha(1\rightarrow4)]_3$	−141	−92.2	−55.8	−91.4	−8.56	−16.1	−15.0	−9.83	−8.71	−10.8
[D-Glcp $\alpha(1\rightarrow4)]_4$	−180	−120	−72.2	−118	−10.7	−21.1	−19.0	−12.1	−10.9	−13.4
[D-Glcp $\alpha(1\rightarrow4)]_5$	−221	−148	−89.1	−146	−12.8	−25.5	−23.1	−14.4	−13.1	−16.2
[D-Glcp $\alpha(1\rightarrow4)]_6$	−260	−175	−105	−172	−15.0	−30.6	−27.2	−16.7	−15.5	−19.0
cyclo[D-Glcp $\alpha(1\rightarrow4)]_5$	−195	−131	−79.6	−131	−11.1	−23.2	−20.2	−12.6	−11.2	−14.1
cyclo[D-Glcp $\alpha(1\rightarrow4)]_6$	−231	−160	−96.5	−158	−12.5	−27.2	−23.7	−14.0	−12.9	−15.8
Δ(cyclic−linear)$_5$	26	17	9.5	15	1.7	2.3	2.9	1.8	1.9	2.1
Δ(cyclic−linear)$_6$	29	15	8.5	14	2.5	3.4	3.5	2.7	2.6	3.2
$\Delta\Delta$(6−5)	3	−2	−1.0	−1	0.8	1.1	0.6	0.9	0.7	1.1
Triton X-100	−34.5	−147	−88.8	−145	19.7	−5.47	9.53	11.4	19.4	20.8
12-Crown-4 ether	−16.9	−39.2	−23.1	−37.3	3.91	−2.68	1.09	0.80	3.58	3.06
15-Crown-5 ether	−21.8	−47.8	−28.6	−46.5	4.55	−3.57	1.19	1.23	4.32	3.78
18-Crown-6 ether	−27.2	−56.6	−34.2	−55.7	5.16	−4.75	1.22	1.64	5.00	4.47
30-Crown-10 ether	−46.6	−95.2	−57.9	−94.1	8.53	−8.40	1.97	3.92	8.34	8.26

* Gibbs free energy of solvation in water (kJ mol^{-1}). † Gibbs free energy of solvation in 1-octanol (kJ mol^{-1}). ‡ Gibbs free energy of solvation in cyclohexane (kJ mol^{-1}). ¶ Gibbs free energy of solvation in chloroform (kJ mol^{-1}). § P_o is the 1-octanol−water partition coefficient. ‖ Calculations carried out with program CDHI. # P_{ch} is the cyclohexane−water partition coefficient. ** Calculations carried out with a method by Leo and Hansch [50]. †† P_{cf} is the chloroform−water partition coefficient.

calculated with SCAP (table 2). The 1-octanol log P_o have been compared with values calculated with CDHI. SCAP P_o decreases monotonically with the number of sugars n in both D-Glcp_n and *cyclo*D-Glcp_n. All the values of log $P_o < -3$, meaning that more than 99.9% of the solute is in the aqueous phase. A negligible quantity of solute is predicted in the organic phase. Even some $-\log P_o$ results are greater than the Avogadro exponent ($P_o < 10^{-23}$). The corresponding interpretation is that no solute molecule would be present in the organic phase to allow experiments for validation. P_o results are of the same order of magnitude as the CDHI computations. This is noticeable because P_o varies in 11 orders of magnitude. Both cyclohexane− and $CHCl_3$−water partition coefficients, P_{ch} and P_{cf}, decrease monotonically with n. The method proposed by Leo and Hansch [50] has been used to compare our results. Some $-\log P$ values are greater than the Avogadro exponent, and no solute molecule would be present in the organic phase. P_{ch} and P_{cf} results are of the same order of magnitude as calculations performed with the method by Leo and Hansch. This is remarkable because P_{ch} and P_{cf} vary in 11−20 orders of magnitude. In particular, the relative error of log P_{cf} is −19%. For the three log P, the difference $\log P_{cyclic} - \log P_{linear}$ is always positive for both D-Glcp_5 and D-Glcp_6. The interpretation is that the macrocycles are less hydrophilic than the linear structures. This is in agreement with the experimental fact that amylose can form single helices with a central channel passing through the molecular axis. In relation to the outside surface the channel is decisively hydrophobic. In particular, the difference $\log P_{cyclic} - \log P_{linear}$ increases from D-Glcp_5 to D-Glcp_6. This means that the decrease of hydrophilicity by cyclation is smaller for D-Glcp_5 than for D-Glcp_6. Triton X-100 and the four crown ethers are amphipathic and their log P_o are rather difficult to calculate and compare. However, the relative errors for log P_{ch} and log P_{cf} are −26 and 10%, respectively.

The AM1 molecular dipole moment μ, ionization potential, electron affinity, volume V and predicted charge transfer for D-Glcp_n are reported in table 3. The helical character of the linear D-Glcp_n increases with n. This is in agreement with the experimental fact that amylose can form single helices. For the linear structures, μ increases smoothly with n until a maximum at $n = 4$. After this value, μ(D-Glcp_5) drops due to the more complete loop of the helix (the whole helical loop requires six sugars). However, on going from D-Glcp_5 to *cyclo* D-Glcp_5 macrocycles, μ is trebled. Both *cyclo*D-Glcp_n exhibit a central cavity of 7.5−8.4 Å width, which is wider than the diameter of thinner SWNTs $d_{t(5,5)} = 6.780$ Å and $d_{t(9,0)} = 7.046$ Å. The positive $EA_{D-Glcp} = 27.5$ kJ mol^{-1} suggests the formation of colloids of positively charged SWNTs in water. This charge transfer is assumed for all D-Glcp_n. Triton X-100 forms colloids of negatively charged SWNTs in water. Although the molecular volume is similar, $\mu_{Triton\,X} = 1.359$D differentiates quantitatively from μ(D-Glcp_n) in the range 2.5−7.3 D. The crown-ether macrocycle 30-crown-10 exhibits a central cavity of *ca.* 8.8 Å width, which is wider than the diameter of thinner SWNTs $d_{t(5,5)} = 6.780$ Å.

Figure 1 shows the variation of the standard heat of formation ΔH_f^o for D-Glcp_n. In particular, for linear D-Glcp_5 the structure is more stable than the corresponding cyclic arrangement. For the linear form, the calculated ΔH_f^o decreases *ca.* 1000 kJ mol^{-1} for each additional sugar. The values correlate linearly with the number of rings n

$$\Delta H_f^o = -234.46 - 999.82n \quad N = 5$$
$$r = 0.99999 \quad s = 6.208 \quad F = 259368.3 \tag{13}$$

The value for D-Glcp_6 extrapolates as $\Delta H_f^o = -6233.4$ kJ mol^{-1} and $\Delta H_f^o/n = -1038.9$ kJ mol^{-1}.

Table 3. Dipole moment, ionization potential, electron affinity, volume and charge transfer for α-(1 → 4)-linked D-glucopyranose residues.

D-glucopyranose residue	μ*	I†	EA‡	V¶	Cavity width§	Charge transfer
D-glucopyranose	2.640	907.1	27.5	153.4	–	$SWNT^+$/co-solvent$^-$
[D-glucopyranose $\alpha(1 \rightarrow 4)]_2$	4.525	–	–	280.9	–	$SWNT^+$/co-solvent$^-$
[D-glucopyranose $\alpha(1 \rightarrow 4)]_3$	4.827	–	–	409.7	–	$SWNT^+$/co-solvent$^-$
[D-glucopyranose $\alpha(1 \rightarrow 4)]_4$	4.889	–	–	537.3	–	$SWNT^+$/co-solvent$^-$
[D-glucopyranose $\alpha(1 \rightarrow 4)]_5$	2.542	–	–	664.7	–	$SWNT^+$/co-solvent$^-$
[D-glucopyranose $\alpha(1 \rightarrow 4)]_6$	–	–	–	793.3	–	$SWNT^+$/co-solvent$^-$
cyclo[D-glucopyranose $\alpha(1 \rightarrow 4)]_5$	7.267	–	–	643.1	7.5	$SWNT^+$/co-solvent$^-$
cyclo[D-glucopyranose $\alpha(1 \rightarrow 4)]_6$	–	–	–	769.1	8.4	$SWNT^+$/co-solvent$^-$
Triton X-100	1.359	–	–	597.7	–	$SWNT^-$/co-solvent$^+$
12-Crown-4 ether	0.000	896.9	−70.6	155.6	4.1	$SWNT^-$/co-solvent$^+$
15-Crown-5 ether	1.710	851.6	−59.1	194.3	5.1	$SWNT^-$/co-solvent$^+$
18-Crown-6 ether	2.390	843.6	−115.3	232.9	6.2	$SWNT^-$/co-solvent$^+$
30-Crown-10 ether	4.363	–	–	388.1	8.8	$SWNT^-$/co-solvent$^+$

* Molecular dipole moment (D) calculated with MOPAC-AM1. † Ionization potential (kJ mol^{-1}) calculated with MOPAC-AM1. ‡ Electron affinity (kJ mol^{-1}) calculated with MOPAC-AM1. ¶ Molecular volume (Å^3). § Cavity width (Å).

Figure 2 shows the variation of the standard heat of formation per unit $\Delta H_f^o/n$ for D-Glc*p* residues. Notice that the shorter chains are relatively more stable than the larger ones. On the other hand, *cyclo*-D-Glcp_5 is relatively less stable than any linear D-Glcp_n. For the linear structures the variation of $\Delta H_f^o/n$ with n fits

$$\frac{1}{\Delta H_f^o/n} = a + \frac{b}{n} \tag{14}$$

where a is the inverse $\Delta H_f^o/n$ of D-Glcp_∞. The calculated $\Delta H_f^o/n$ turns out to be

$$\frac{1}{\Delta H_f^o/n} = -0.0009895 + \frac{0.0001817}{n} \tag{15}$$

$$N = 5 \quad r = 0.999 \quad s = 3.2 \times 10^{-6} \quad F = 1393.8$$

and $\Delta H_f^o/n$ for D-Glcp_∞ extrapolates as $-1010.6\,\mathrm{kJ\,mol^{-1}}$. The value for D-Glc$p_6$ extrapolates as $\Delta H_f^o/n = -1042.5\,\mathrm{kJ\,mol^{-1}}$, in agreement with $-1038.9\,\mathrm{kJ\,mol^{-1}}$ obtained from the extrapolation of figure 1.

Amylose forms the well-known dark-blue stained amylose–iodine complex. The variation of ΔH_f^o has been calculated for the following I_n^{z-} anions: I_3^-, I_5^-, I_6^{2-}, I_8^{2-}, I_{10}^{2-} and I_{11}^{3-}. In particular, I_6^{2-} and I_{11}^{3-} are less stable than the general trend. For the remaining anions, the calculated ΔH_f^o decreases *ca.* $22\,\mathrm{kJ\,mol^{-1}}$ for each additional iodine atom/anion. Figure 3 displays the variation of $\Delta H_f^o/n$ for I_n^{z-} anions. In general, the shorter chains are relatively more stable than the larger ones. Again I_6^{2-} and I_{11}^{3-} are relatively less stable. For the remaining anions the calculated $\Delta H_f^o/n$ turns out to be

$$\frac{1}{\Delta H_f^o/n} = -0.0356 + \frac{0.0574}{n} \tag{16}$$

$$N = 4 \quad r = 0.989 \quad s = 0.001 \quad F = 89.7$$

and $\Delta H_f^o/n$ for I_∞^{z-} extrapolates as $-28.1\,\mathrm{kJ\,mol^{-1}}$. The AM1 ΔH^o of the D − Glc*p*/I_m^- interaction is −67.1, −54.6, −81.8, −69.6, −63.2 and $-79.1\,\mathrm{kJ\,mol^{-1}}$ for D − Glc*p*·I_3^-, D − Glc*p*·I_5^-, D − Glc*p*·I_6^{2-}, D − Glc*p*·I_8^{2-}, D − Glc*p*·I_{10}^{2-} and D − Glc*p*·I_{11}^{3-}, respectively. All the values lie in the experimental range for the amylose/iodine interaction is from −87 to $-42\,\mathrm{kJ\,mol^{-1}}$ [51]. This is in agreement with the experimental fact that amylose can

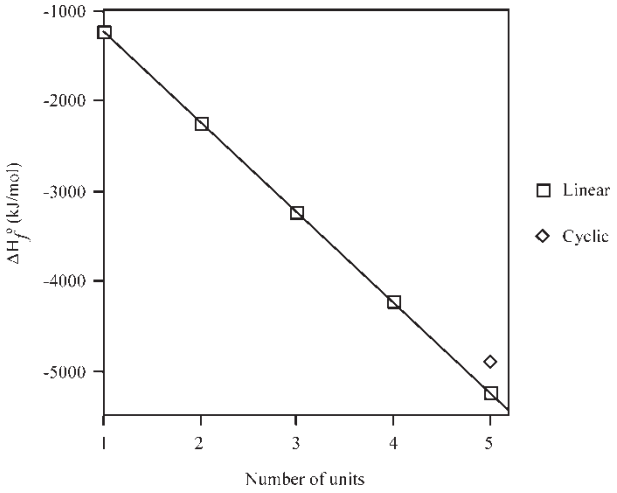

Figure 1. MOPAC-AM1 standard heat of formation for D-Glcp_n vs. number of units.

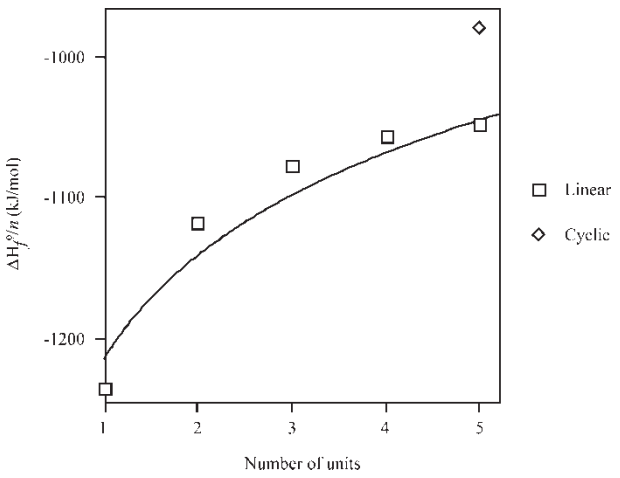

Figure 2. MOPAC-AM1 standard heat of formation per unit for D-Glcp_n vs. number of units.

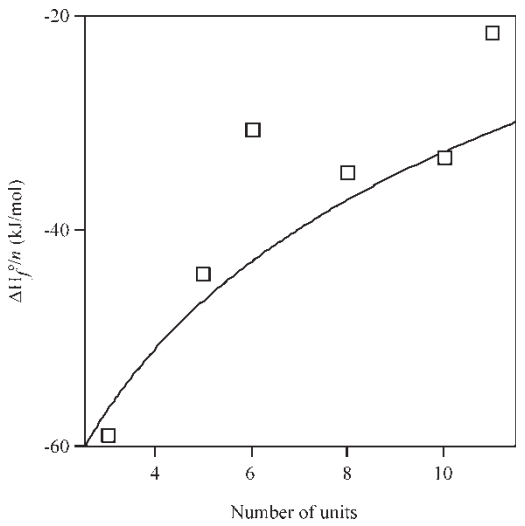

Figure 3. MOPAC-AM1 standard heat of formation per unit for I_n^{z-} vs. number of units.

form inclusion complexes, e.g. with fatty acids [52] and iodine. In the well-known dark-blue stained amylose–iodine complex, the channel structure serves as a well-ordered matrix to accommodate nearly linear polyiodide chains with an almost perfect steric fit [53]. Helical D-Glcp_n exhibits a central channel of *ca.* 5.4 Å width. Formation of the D-Glcp_n-iodine–iodide complex is paralleled by a slight expansion of the diameter of the helix [54]. On the basis of thinner SWNT diameters $d_{t(5,5)} = 6.780$ Å, an expansion is suggested for the helical D-Glcp_n–SWNT complexes.

4. Conclusions

The following conclusions can be made from this study.

1. Solubility of SWNTs has been investigated in a variety of solvents, finding a class of non-hydrogen-bonding Lewis bases that provide good solubility. Solvents have been grouped into three classes. SWNTs in some organic solvents are positively charged, while in water/Triton X are negative. Categorized solubility has been semiquantitatively correlated with solvent parameters.
2. *Cyclo*D-Glcp_n are less hydrophilic than linear structures. The decrease of hydrophilicity by cyclation is smaller for D-Glcp_5 than for D-Glcp_6. The lipophilicity characteristics of *cyclo*D-Glcp_n point towards the hydrophobic effect as an important factor governing the formation of D-Glcp_n-inclusion complexes with hydrophobic molecules by incorporation into the hydrophobic channel.
3. The positive electron affinity of D-Glc$p$ suggests the formation of colloids of positively charged SWNTs in water. This charge transfer is assumed for all D-Glcp_n.
4. Variation of $\Delta H_f^\circ/n$ for D-Glcp_n shows that shorter chains are more stable than larger ones. *Cyclo*D-Glcp_n are less stable than linear D-Glcp_n. Variation of $\Delta H_f^\circ/n$ for I_n^{z-} indicates that shorter chains are more stable than larger ones. An expansion of the central channel is suggested for the helical D-Glcp_n–SWNT complexes.

Work is in progress on the study of D − Glcp_n·I_m^{z-}, D-Glcp_n–SWNT and crown ether–SWNT complexes. This would give an insight into a possible generality of these conclusions.

Acknowledgements

The author acknowledges financial support from the Spanish MCT (Plan Nacional I + D + I, Project No. BQU2001-2935-C02-01) and Generalitat Valenciana (DGEUI Project Nos. INF01-051 and INFRA03-047).

References

[1] S. Iijima, T. Ichihashi. Single-shell carbon nanotubes of 1-nm diameter. *Nature*, **363**, 603 (1993).
[2] P.M. Ajayan. Nanotubes from carbon. *Chem. Rev.*, **99**, 1787 (1999).
[3] R.J. Chen, Y. Zhang, D. Wang, H. Dai. Noncovalent sidewall functionalization of single-walled carbon nanotubes for protein immobilization. *J. Am. Chem. Soc.*, **123**, 3838 (2001).
[4] J. Chen, M.A. Hamon, H. Hu, Y. Chen, A.M. Rao, P.C. Eklund, R.C. Haddon. Solution properties of single-walled carbon nanotubes. *Science*, **282**, 95 (1998).
[5] P.J. Boul, J. Liu, E.T. Mickelson, C.B. Huffman, L.M. Ericson, I.W. Chiang, K.A. Smith, D.T. Colbert, R.H. Hauge, J.L. Margrave, R.E. Smalley. Reversible sidewall functionalization of buckytubes. *Chem. Phys. Lett.*, **310**, 367 (1999).
[6] A. Star, J.F. Stoddart, D. Steuerman, M. Diehl, A. Boukai, E.W. Wong, X. Yang, S.-W. Chung, H. Choi, J.R. Heath. Preparation and properties of polymer-wrapped single-walled carbon nanotubes. *Angew. Chem., Int. Ed. Engl.*, **40**, 1721 (2001).
[7] M. Yudasaka, M. Zhang, C. Jabs, S. Iijima. Effect of an organic polymer in purification and cutting of single-wall carbon nanotubes. *Appl. Phys. A*, **71**, 449 (2001).
[8] M.J. O'Connell, P. Boul, L.M. Ericson, C. Huffman, Y. Wang, E. Haroz, C. Kuper, J. Tour, K.D. Ausman, R.E. Smalley. Reversible water-solubilization of single-walled carbon nanotubes by polymer wrapping. *Chem. Phys. Lett.*, **342**, 265 (2001).
[9] G.S. Duesberg, J. Muster, V. Krstic, M. Burghard, S. Roth. Chromatographic size separation of single-wall carbon nanotubes. *Appl. Phys. A*, **67**, 117 (1998).
[10] D.B. Thompson. On the non-random nature of amylopectin branching. *Carbohyd. Polym.*, **43**, 223 (2000).
[11] F. Diederich, M. Gómez-López. Supramolecular fullerene chemistry. *Chem. Soc. Rev.*, **28**, 263 (1999).
[12] Á. Buvári-Barcza, J. Rohonczy, N. Rozlosnik, T. Gilányi, B. Szabó, G. Lovas, T. Braun, J. Samu, L. Barcza. Aqueous solubilization of [60]fullerene *via* inclusion complex formation and the hydration of C_{60}. *J. Chem. Soc., Perkin Trans.*, **2**, 191 (2001).
[13] V.T. D'Souza, K.B. Lipkowitz. Cyclodextrins: introduction. *Chem. Rev.*, **98**, 1741 (1998).
[14] A. Star, D.W. Steuerman, J.R. Heath, J.F. Stoddart. Starched carbon nanotubes. *Angew. Chem., Int. Ed. Engl.*, **41**, 2508 (2002).
[15] G. Wenzt. Cyclodextrins as building blocks for supramolecular structures and functional units. *Angew. Chem., Int. Ed. Engl.*, **33**, 803 (1994).
[16] F. Torrens. Table of periodic properties of the fullerenes based on structural parameters. *J. Chem. Inf. Comput. Sci.*, **44**, 60 (2004).
[17] F. Torrens. Table of periodic properties of fullerenes based on structural parameters, *J. Mol. Struct.* (Theochem), in press.
[18] F. Torrens. Periodic table of carbon nanotubes based on the chiral vector, *Internet Electron. J. Mol. Des.*, **3**, 514 (2004).
[19] F. Torrens. Periodic properties of carbon nanotubes based on the chiral vector, *Internet Electron. J. Mol. Des.*, in press.

[20] F. Torrens. Calculations on organic-solvent dispersions of single-wall carbon nanotubes, *Int. J. Quantum Chem.*, in press.
[21] F. Torrens, E. Ortí, J. Sánchez-Marín. Vectorized TOPO program for the theoretical simulation of molecular shape. *J. Chim. Phys. Phys.-Chim. Biol.*, **88**, 2435 (1991).
[22] A. Bondi. Van der Waals volumes and radii. *J. Phys. Chem.*, **68**, 441 (1964).
[23] A.Y. Meyer. Molecular mechanics and molecular shape. Part 1. Van der Waals descriptors of simple molecules. *J. Chem. Soc., Perkin Trans.*, **2**, 1161 (1985).
[24] F. Torrens, J. Sánchez-Marín, I. Nebot-Gil. New dimension indices for the characterization of the solvent-accessible surface. *J. Comput. Chem.*, **22**, 477 (2001).
[25] M. Lewis, D.C. Rees. Fractal surfaces of proteins. *Science*, **230**, 1163 (1985).
[26] D.R. Flower. SERF: a program for accessible surface area calculations. *J. Mol. Graphics Mod.*, **15**, 238 (1997).
[27] F. Torrens, M. Rubio, J. Sánchez-Marín. AMYR 2: a new version of a computer program for pair potential calculation of molecular associations. *Comput. Phys. Commun.*, **115**, 87 (1998).
[28] B. Terryn, J. Barriol. On the evaluation of the usual quantities or coefficients related to the shape of a molecule approximated on the basis of the van der Waals radii. *J. Chim. Phys. Phys.-Chim. Biol.*, **78**, 207 (1981).
[29] J.L. Pascual-Ahuir, E. Silla, J. Tomasi, R. Bonaccorsi. Electrostatic interaction of a solute with a continuum. Improved description of the cavity and of the surface cavity bound charge distribution. *J. Comput. Chem.*, **8**, 778 (1987).
[30] F. Torrens, J. Sánchez-Marín, I. Nebot-Gil. Universal model for the calculation of all organic solvent–water partition coefficients. *J. Chromatogr. A*, **827**, 345 (1998).
[31] F. Torrens. Universal organic solvent–water partition coefficient model. *J. Chem. Inf. Comput Sci.*, **40**, 236 (2000).
[32] F. Torrens. Calculation of partition coefficient and hydrophobic moment of the secondary structure of lysozyme. *J. Chromatogr. A*, **908**, 215 (2001).
[33] F. Torrens. Free energy of solvation and partition coefficients in methanol–water binary mixtures. *Chromatographia*, **53**, S199 (2001).
[34] F. Torrens. Calculation of organic solvent–water partition coefficients of iron–sulphur protein models. *Polyhedron*, **21**, 1357 (2002).
[35] F. Torrens, V. Soria. Stationary–mobile phase distribution coefficient for polystyrene standards. *Sep. Sci. Technol.*, **37**, 1653 (2002).
[36] A.J. Hopfinger. Polymer–solvent interactions for momopolypeptides in aqueous solution. *Macromolecules*, **4**, 731 (1971).
[37] M. Born. Volume and heat of hydration of ions. *Z. Phys.*, **1**, 45 (1920).
[38] A.A. Maryott, E.R. Smith. *Table of Dielectric Constants of Pure Liquids, National Bureau of Standards Circular No. 514*, United States Department of Commerce-National Bureau of Standards, Washington (1951).
[39] A. Kantola, H.O. Villar, G.H. Loew. Atom based parametrization for a conformationally dependent hydrophobic index. *J. Comput. Chem.*, **12**, 681 (1991).
[40] S. Fraga. A semiempirical formulation for the study of molecular interactions. *J. Comput. Chem.*, **3**, 329 (1982).
[41] J. Gasteiger, M. Marsili. Iterative partial equalization of orbital electronegativity: a rapid access to atomic charges. *Tetrahedron*, **36**, 3219 (1980).
[42] F. Torrens. Effect of type, size and deformation on polarizability of carbon nanotubes from atomic increments. *Nanotechnology*, **15**, S259 (2004).
[43] M.J.S. Dewar, E.G. Zoebisch, E.F. Healy, J.J.P. Stewart. AM1: a new general purpose quantum mechanical molecular model. *J. Am. Chem. Soc.*, **107**, 3902 (1985).
[44] K.D. Ausman, R. Piner, O. Lourie, R.S. Ruoff, M. Korobov. Organic solvent dispersions of single-walled carbon nanotubes: toward solutions of pristine nanotubes. *J. Phys. Chem. B*, **104**, 8911 (2000).
[45] M.J. Kamlet, R.W. Taft. The solvatochromic comparison method. I. The β-scale of solvent hydrogen-bond acceptor (HBA) basicities. *J. Am. Chem. Soc.*, **98**, 377 (1976).
[46] R.W. Taft, M.J. Kamlet. The solvatochromic comparison method. 2. The α-scale of solvent hydrogen-bond donor (HBD) acidities. *J. Am. Chem. Soc.*, **98**, 2886 (1976).
[47] M.J. Kamlet, J.L. Abboud, R.W. Taft. The solvatochromic comparison method. 6. The π^* scale of solvent polarities. *J. Am. Chem. Soc.*, **99**, 6027 (1977).
[48] M.V. Korobov, A.L. Mirakyan, N.V. Avramenko, G. Olofsson, A.L. Smith, R.S. Ruoff. Calorimetric studies of solvates of C_{60} and C_{70} with aromatic solvents. *J. Phys. Chem. B*, **103**, 1339 (1999).
[49] M.R. Diehl, S.N. Yaliraki, R.A. Beckman, M. Barahona, J.R. Heath. Self-assembled, deterministic carbon nanotube wiring networks. *Angew. Chem., Int. Ed. Engl.*, **41**, 353 (2002).
[50] A. Leo, C. Hansch. Linear free-energy relationships between partitioning solvent systems. *J. Org. Chem.*, **36**, 1539 (1971).
[51] T. Handa, H. Yajima, T. Yamamura, T. Ishii, H. Aikawa. *Stärke/Starch*, **32**, 194 (1980).
[52] M.A. Rutschmann, J. Solms. Formation of inclusion complexes of starch with different organic compounds. IV. Ligand binding and variability in helical conformations of V amylose complexes. *Lebensm.-Wiss. Technol.*, **23**, 84 (1990).
[53] T.L. Bluhm, P. Zugenmaier. *Carbohyd. Res.*, **89**, 1 (1981).
[54] T. Hirai, M. Hirai, S. Hayashi, T. Ueki. Study of the conformational change of amylose induced by complexation with iodine using synchrotron X-ray small-angle scattering. *Macromolecules*, **25**, 6699 (1992).